# THE WIDE-BAND PLASMA WAVE INVESTIGATION

D. A. Gurnett, R. L. Huff, and D. L. Kirchner
Department of Physics and Astronomy
The University of Iowa
Iowa City, IA  52242  U.S.A.

**Abstract**.  As part of the Cluster Wave Experiment Consortium (WEC), the Wide-Band (WBD) Plasma Wave investigation is designed to provide high-resolution measurements of both electric and magnetic fields in selected frequency bands from 25 Hz to 577 kHz.  Continuous waveforms are digitised and transmitted in either a 220 kbit/s real-time mode or a 73 kbit/s recorded mode.  The real-time data are received directly by a NASA Deep-Space Network (DSN) receiving station, and the recorded data are stored in the spacecraft solid-state recorder for later playback.  In both cases the waveforms are Fourier transformed on the ground to provide high-resolution frequency-time spectrograms.  The WBD measurements complement those of the other WEC instruments and also provide a unique new capability for performing very-long-baseline interferometry (VLBI) measurements.

## I.        Introduction

The Cluster Wide-Band (WBD) Plasma Wave investigation is designed to provide very high-resolution frequency-time measurements of plasma waves in the Earth's magnetosphere.  The WBD instrumentation is part of the Wave Experiment Consortium (WEC) and consists of a digital wide-band receiver that can provide electric- or magnetic-field waveforms over a wide range of frequencies.  Wide-band receivers have played an important role in many previous spacecraft missions, including GEOS, ISEE, Voyager, DE and Galileo.  The WBD instruments on the four Cluster spacecraft are similar in design to those being flown on the Polar and Cassini spacecraft.  The investigators responsible for the WBD investigation on Cluster are listed in Table I.

The wide-band technique involves transmitting band-limited waveforms directly to the ground using a high-rate data link.  The primary advantage of this approach is that continuous waveforms are available for detailed high-resolution frequency-time analyses.  The frequency-time resolution is limited only by the uncertainty principle, $\Delta\omega\Delta t \sim 1$.  Since the frequency resolution ($\Delta\omega$) and time resolution ($\Delta t$) can be selected on the ground, the wide-band technique has the advantage that the resolution can be adjusted to provide optimum analysis of the phenomena of interest.

**Table I.  Cluster WBD Investigators**

| Principal Investigator | Affiliation |
|---|---|
| Donald A. Gurnett | The University of Iowa |
| **Co-Investigators** | |
| Jean-Louis H. Bougeret | Observatoire de Paris (Meudon) |
| Patrick Canu | Centre d'etudes des Environnements Terrestre et Planetaires/UVSQ |
| Georg Gustafsson | Swedish Inst. of Space Physics |
| Gerhard Haerendel | Max-Planck-Institut für extraterrestriche Physik |
| Robert A. Helliwell | Stanford University |
| Umran S. Inan | Stanford University |
| Warren L. Martin | Jet Propulsion Laboratory |
| Robert L. Mutel | The University of Iowa |
| Bent Pedersen | Observatoire de Paris (Meudon) |
| Alain Roux | Centre d'etudes des Environnements Terrestre et Planetaires/UVSQ |
| Steven R. Spangler | The University of Iowa |
| Eigil Ungstrup | Geophysical Institute (Copenhagen) |
| Les Woolliscroft* | The University of Sheffield |

*Deceased.

The high-resolution nature of wide-band measurements is particularly important for the study of plasma emissions that have very complex frequency-time characteristics.  To illustrate the flexibility and high resolution available from wide-band data, Figure 1 shows representative spectrograms of several types of plasma wave emissions that are commonly observed in the Earth's magnetosphere.  The spectrogram in panel (a), for example, has been processed using a very expanded time scale to resolve the fine structure of whistler-mode chorus emissions.  Chorus is an electromagnetic emission that propagates in the whistler mode at frequencies below the electron cyclotron frequency [Helliwell, 1965].  These emissions are believed to be produced by energetic electrons trapped in the terrestrial radiation belts [Kennel and Petschek, 1966].  The spectrogram in panel (b) has been processed with greatly expanded frequency resolution at low frequencies to resolve the narrow-band structure of electrostatic ion cyclotron waves.  Electrostatic ion cyclotron waves are electrostatic waves that propagate near harmonics of the ion cyclotron frequency [Kintner et al., 1978].  These waves are believed to be excited by field-aligned currents, and by highly anisotropic low-energy ion distributions.  The spectrograms in panels (c) and (d) were obtained in a frequency conversion mode of operation and show the extremely complicated fine structure of $(n + 1/2)f_c$ electron cyclotron waves near the upper hybrid resonance (UHR) and the complex narrow-band structure of auroral kilometric radiation.  The $(n + 1/2)f_c$ electron cyclotron waves are electrostatic waves that occur between harmonics of the electron cyclotron frequencies.  These waves are believed to be excited by highly anisotropic low-energy electron distributions [Ashour-Abdalla and Kennel, 1978].  Auroral kilometric radiation is an intense electromagnetic emission generated in the Earth's auroral regions [Gurnett, 1974].
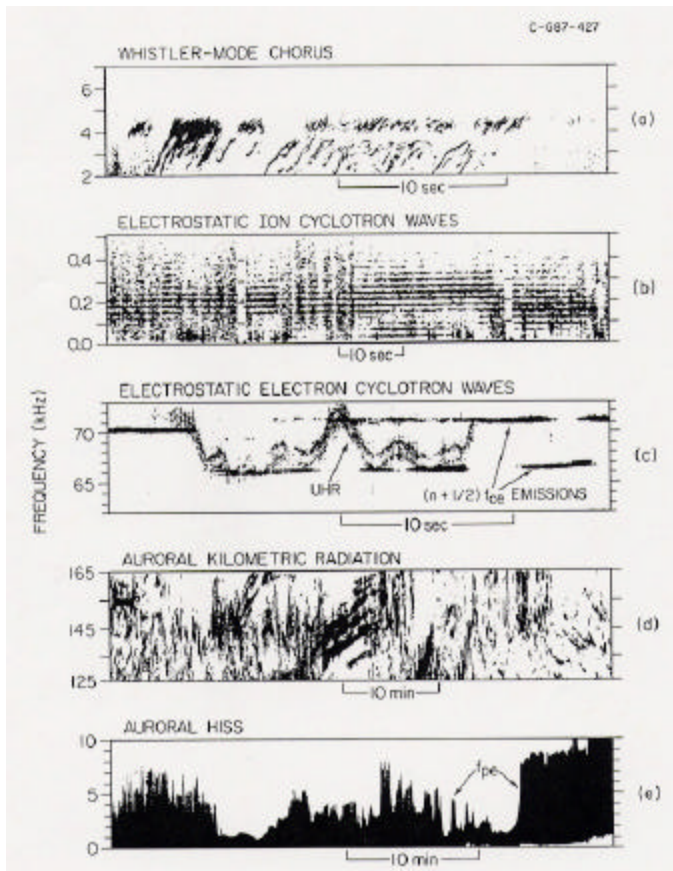
**Figure 1.** Frequency-time spectrograms of plasma emissions observed in the Earth's magnetosphere using wide-band instrumentation.

These emissions often have an extremely complex fine structure [Gurnett et al., 1979]. Finally, to illustrate the use of wide-band data as a means for obtaining very high-resolution measurements of basic plasma parameters, panel (e) shows a spectrum of auroral hiss that has a sharp upper frequency cutoff at the electron plasma frequency, $f_{pe}$. The cutoff at $f_{pe}$ provides very accurate (few percent), high resolution (0.1 s) measurements of electron densities in the auroral zone and over the polar cap [Persoon et al., 1983].

## 2. Scientific Objectives

The eccentric, highly inclined orbit of the Cluster spacecraft carries the spacecraft through most of the important regions of the magnetosphere, including the polar cusp, the plasma mantle, the magnetopause boundary layer, the polar cap, the auroral zones, the plasma sheet, and the plasma sheet boundary layer. Many different types of plasma waves occur in these regions. Some of the more important include electrostatic ion cyclotron waves, whistler-mode chorus, auroral hiss, auroral kilometric radiation, continuum radiation, electrostatic electron cyclotron waves, upper hybrid waves, and lower hybrid waves.

Within the Wave Experiment Consortium, each experiment has its own areas of specialisa-tion as described in the WEC overview (see Pedersen *et al.*, this issue) and the WEC companion papers. The primary purpose of the WBD investigation is to support WEC science objectives by providing high-resolution spectral analysis. At boundaries and other regions with steep spatial gradients, WBD provides high-time resolution single-spacecraft measurements for comparison with data from other instruments, such as the magnetometer and plasma instruments. From these data, waves produced by current-driven instabilities and

other mechanisms involving spatial inhomogeneities can be clearly identified.  In addition to single-point measurements, wide-band data from two or more spacecraft can also be used to resolve space! time ambiguities as the spacecraft pass through complex spatial structures.  The study of such structures is one of the primary objectives of the Cluster mission.  In cases where the upper hybrid frequency or electron plasma frequency can be identified, WBD can also provide very high resolution mea-surements of the electron density.  Also, multiple-point comparisons of electron densities can be used to analyse the motion and evolution of plasma structures in the auroral zone and polar cap.

A-G87-407-2
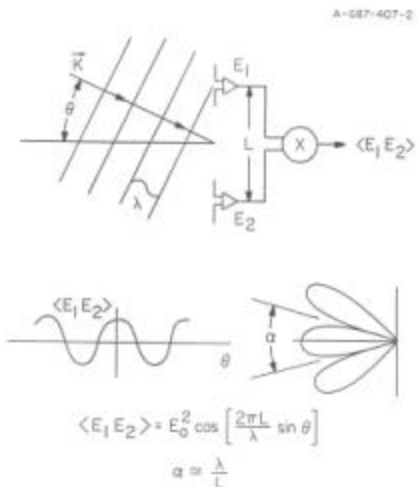
**Figure 2.**    The angular response of a two-point radio interferometer.  The response consists of a series of lobes, each with a beamwidth, $\alpha = \lambda/L$.

$$\langle E_1 E_2 \rangle = E_0^2 \cos\left[\frac{2\pi L}{\lambda}\sin\theta\right]$$

$$\alpha = \frac{\lambda}{L}$$

In addition to providing measurements that support the overall objectives of the WEC, the WBD instrument can be used to provide multi-spacecraft long-baseline radio interferometry measurements.  The basic principles of a radio interferometer are illustrated in Figure 2 which shows an electromagnetic wave of wavelength $\lambda$ incident on two antennas separated by a baseline distance $L$.  The signals from the two antennas, $E_1$ and $E_2$, are multiplied and averaged to produce a cross-correlation $\langle E_1 E_2 \rangle$.  The sign and amplitude of the cross-correlation is determined by the angle of arrival $\theta$ relative to the symmetry axis of the interferometer.  If the wavelength of the radiation is less than the separation distance between the antennas, then the cross-correlation varies as the cosine of the angle of arrival.  The antenna pattern of the interferometer then has a series of lobes, each with a beamwidth $\alpha$.  If a source moves through this fan-shaped antenna pattern, a sinusoidal "fringe" pattern is produced in the cross-correlation.

Two-point interferometry measurements of the type described above have been performed by the ISEE spacecraft (Baumback *et al.,* 1986).  Figure 3 shows simultaneous observations of auroral kilometric radiation from the ISEE-1 and -2 spacecraft at a geocentric radial distance of about 14 $R_E$, and a baseline separation distance of 3,260 km.  The top two panels show the auroral kilometric radiation spectrum received at the two spacecraft, and the bottom panel shows
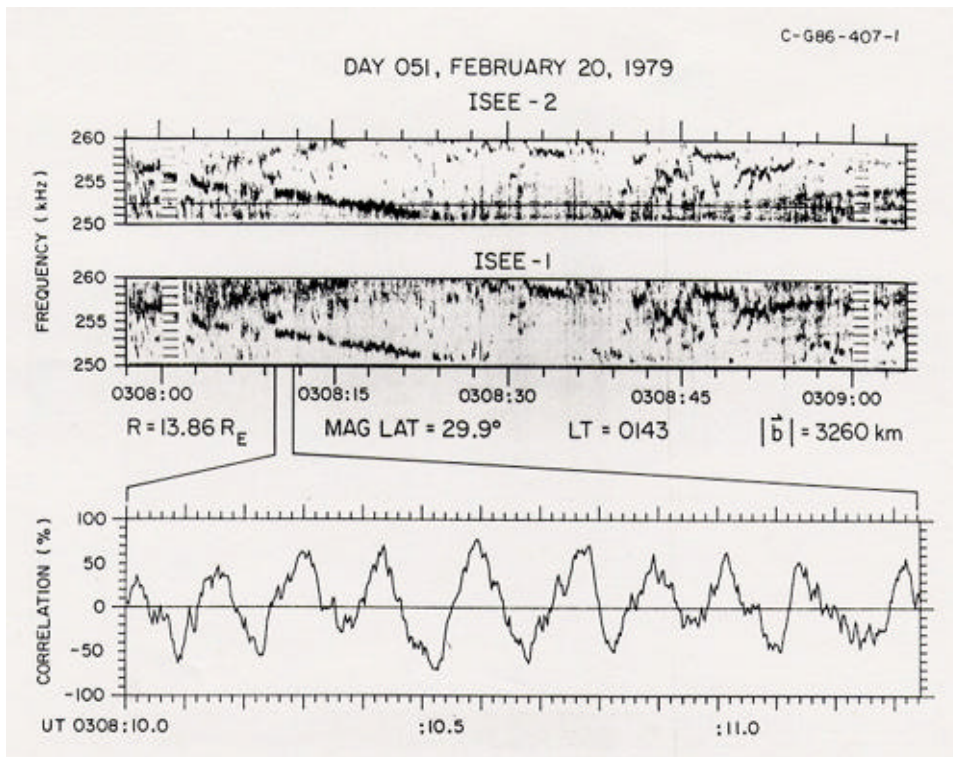
**Figure 3.** Simultaneous frequency-time spectrograms of an auroral kilometric radiation event detected by ISEE-1 and -2. The bottom panel shows an interference fringe pattern in the cross-correlation between the two signals.

a plot of the cross-correlation on an expanded time scale that covers a time interval of about 1.3 s. The sinusoidal waveform in the cross-correlation is the characteristic "fringe pattern" produced by interference between the two received signals. By analysing the fringe amplitude, the angular size of the source can be determined. An important parameter in any interferometer experiment is the number of baseline separations involved between the various antennas. With ISEE-1 and -2 only one baseline was available, which meant that only one component of the source brightness distribution could be studied. With Cluster a total of six baselines can be achieved between the four spacecraft. Up to ten baselines can be obtained if simultaneous measurements are obtained between Cluster and the Polar spacecraft (Gurnett *et al.*, 1995), which has a similar wide-band receiver. Multi-spacecraft interferometer measurements have the potential of giving important new information on the angular motion and size of various terrestrial and astronomical radio sources.

### 3. Description of the Wide-Band Receiver System

A simplified block diagram of the WBD instrument is shown in Figure 4. The instrument processes signals from four antennas, any one of which can be chosen via the antenna selection switch located at the input to the receiver. The four selectable inputs consist of two electric-field signals ($E_y$ and $E_z$), and two magnetic-field signals ($B_x$ and $B_y$). These inputs are provided by the electric-field (EFW) and magnetic-field (STAFF) experiments. Unregulated power is supplied to WBD by the WEC power supply. Power switching and all commands to the WBD are provided by the WEC data-processing unit (DWP). The WBD electronics are enclosed in a gold-plated magnesium housing. A photograph of WBD Flight Model 3 is shown in Figure 5. A

summary of WBD instrument parameters is given in Table II. Individual aspects of the wide-band receiver system are discussed in detail in the following sections.
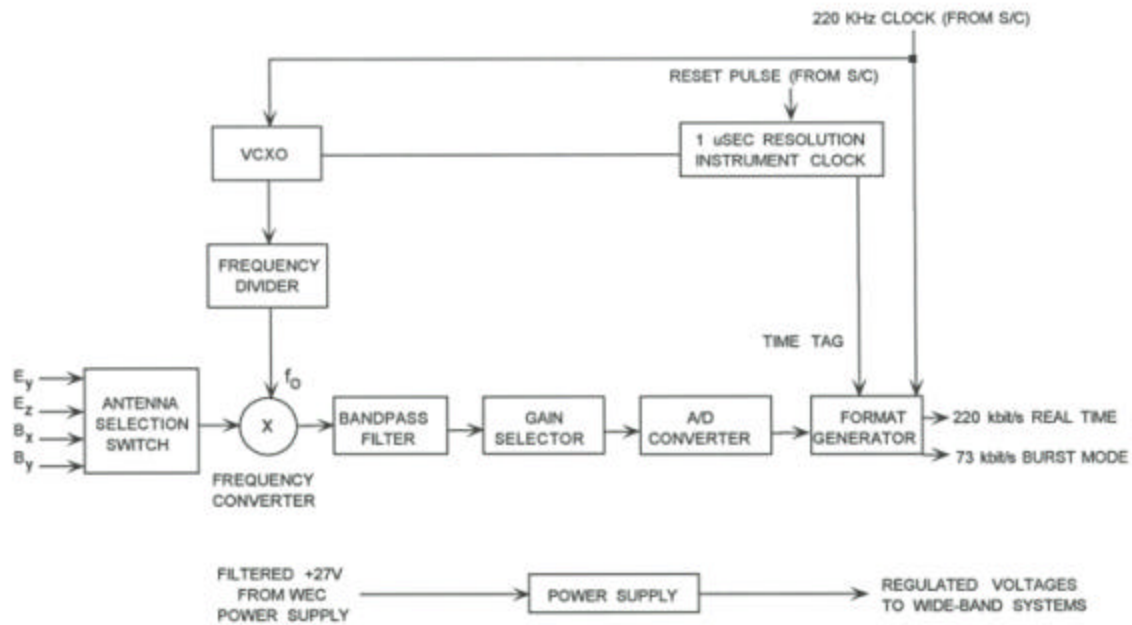


**Figure 4.** Block diagram of the Cluster wide-band receiver.



**Figure 5.** WBD Flight Model 3.

**Table II.  WBD Instrument Parameters**

| Sensors | Two electric-field components ($E_y$, $E_z$); two magnetic-field components ($B_x$,$B_y$) |
|---|---|
| Conversion Frequencies | 0, 125 kHz, 250 kHz, 500 kHz |
| Bandpass Filter Ranges | 1 kHz to 77 kHz<br>50 Hz to 19 kHz<br>25 Hz to 9.5 kHz |
| Frequency Resolution | Determined by FFT |
| Time Resolution | 10-20 msec (per FFT spectrum) |
| Gain Select | 5 dB steps, 16 levels, dynamic range 75 dB, automatic ranging or set by command |
| A/D Converter | 1-bit, 4-bit, or 8-bit resolution for a selection of sample rates |
| Mass (flight models, measured) | 1.67 kg |
| Power (flight models, measured) | 1.57 W |

## 3.1  SENSORS AND SENSOR INTERFACES

The Cluster plasma-wave sensors consist of two orthogonal spherical electric antennas located in the spin plane of the spacecraft, and a triaxial search coil magnetometer oriented with two axes in the spin plane and the third axis parallel to the spacecraft spin axis.  The electric antennas, designated $E_y$ and $E_z$, are provided by the EFW investigation and have sphere-to-sphere separations of 100 m when fully deployed.  The spheres each contain a high-impedance preamplifier that provides signals to the EFW main electronics, to the WBD, and to the other wave instruments via buffer amplifiers.  The EFW/WBD buffer amplifier is a low-noise, low-power design that maintains a flat response up to about 600 kHz.  The boom-mounted three-axis search coil magnetometer ($B_x$, $B_y$, and $B_z$) is part of the STAFF instrumentation, and provides magnetic-field measurements up to 4 kHz.  The WBD instrument has the capability of processing signals from only one of the four sensors.  The sensor selection is controlled by spacecraft command via the DWP.

## 3.2  FREQUENCY BANDS

The input frequency range of the wide-band receiver can be shifted by a frequency converter to any one of four frequency ranges, where the conversion frequency, $f$, determines the lower edge of the frequency range selected.  The conversion frequency is obtained by dividing a 14-MHz reference oscillator that is located within the WBD instrument.  To maintain phase stability in the entire system, this oscillator is synchronised to the spacecraft 220.752-kHz high-frequency clock.  The high-frequency clock is obtained by dividing the spacecraft Ultra-Stable Oscillator (USO).  The USO operates at a frequency of $2^{23}$ Hz with a stability ($\Delta f/f$) of 6.5 H $10^{-9}$ over a 12-hour period.

A spacecraft command to select a particular frequency band causes DWP to switch the wide-band receiver to an appropriate input bandpass filter and to a conversion frequency of either 0, 125, 250, or 500 kHz.  If baseband ($f$=0) is selected, the mixing stage is bypassed so that the signal is routed directly to the output with no frequency conversion.

The bandwidth of the WBD output waveform is determined by one of three bandpass filters selected in combination with a given output mode.  The conversion frequencies and bandpass filter ranges are summarised in Table II .

### 3.3  GAIN CONTROL

The gain of the wide-band receiver is determined by a set of four dual-gain amplifiers that may be selected to provide various gains in increments of 5 dB.  The dual-gain amplifiers have gains of 0 or 5 dB, 0 or 10 dB, 0 or 20 dB, and 0 or 40 dB.  The gain control has two modes of operation:  fixed and auto-ranging.  The gain control modes are controlled by spacecraft command.

In the fixed-gain mode, the receiver gain can be set to any one of the sixteen levels (from 0 dB to 75 dB).  In the auto-ranging mode, the output from the programmable amplifier is compared to a pair of reference amplitudes.  If the criteria for changing the gain are met, the gain is either increased by one step (5 dB) or decreased by one step.  In order to avoid excessive toggling between gain steps, a commandable threshold must be exceeded, thereby introducing hysteresis in the Automatic Gain Control (AGC) loop.  The gain is updated at a rate determined by the gain update clock, which is a DWP function selected by spacecraft command.  The period of the clock is programmable from 0.1 to 27 s in increments of 0.1 s.  The actual gain change takes place at the beginning of the next WBD major frame.

### 3.4  A/D CONVERTER AND FORMAT GENERATOR

The output analogue waveform is sampled by an 8-bit analogue-to-digital converter that provides the sampling resolution and data output rates listed in Table III.  For sample rates where the bit rate exceeds the spacecraft telemetry rate (220 kbit/s), the digitised wide-band data is duty-cycled by a format generator that reduces the average bit rate to 220 kbit/s.  The format generator organises the digitised waveform data into a 1096-byte output frame, which includes appropriate timing and status information.

### Table III.  WBD Output Modes

| Mode | Bandwidth | Sample Rate | Bits/ Sample | Duty Cycle | Comments |
|---|---|---|---|---|---|
| 0 | 25 Hz - 9.5 kHz | 27.4 kHz | 8 | 100% | Default Mode |
|  | 25 Hz - 9.5 kHz | 27.4 kHz | 8 | 100% |  |
| 2 | 50 Hz - 19 kHz | 54.9 kHz | 4 | 100% |  |
| 3 | 50 Hz - 19 kHz | 54.9 kHz | 8 | 50% |  |
| 4 | 1 kHz - 77 kHz | 219.5 kHz | 8 | 12.5% |  |
| 5 | 1 kHz - 77 kHz | 219.5 kHz | 1 | 100% |  |
| 6 | 1 kHz - 77 kHz | 219.5 kHz | 4 | 25% |  |
| 7 | 1 kHz - 77 kHz | 219.5 kHz | 8 | 12.5% | *Note 1 |

*Note 1.      This mode is a repeat of output Mode 4, but also toggles the primary and redundant OBDH interfaces

## *3.5*     *WBD DATA INTERFACE*

The WBD instrument utilises two separate paths for transferring frames of digitised waveform data to the spacecraft data-handling system.  The primary path supports real-time acquisition of WBD data by the NASA DSN.  The secondary path supports non-real-time data acquisition via the spacecraft solid-state recorder.

### 3.5.1  *Real-Time Data Acquisition*
A special serial data interface between the WEC and the spacecraft Central Data Management Unit (CDMU) supplies the primary path for data from the WBD instrument.  The interface functions consist of a 220 kHz sampling clock, a timing pulse, and the data output.  These interfaces are all redundant. Data are present at this interface whenever WBD is powered.  During real-time data acquisition (TDA Mode 8), the WBD data appears on a dedicated virtual telemetry channel (VC5), embedded in the 1096-byte data field of the standard 1279-byte transfer frame.  The WBD transfer frames are acquired by a DSN receiving station.

### 3.5.2   *Non-Real-Time Data Acquisition*
The secondary path for the WBD data is provided by a serial interface between WBD and DWP.  This interface supports a non-real-time time mode of data collection (TDA Mode 5.2, or BM2) dedicated mainly to WBD.  When the BM2 operational mode is enabled, WBD data are transferred to DWP at 220 kbit/s, and the DWP, in turn, reduces the wide-band data by a factor of three either by digital filtering or duty cycling (accepting only one out of three frames).  At the new average bit rate of 73 kbit/s, the WBD data are transferred to the On-Board Data-Handling (OBDH) system for recording and subsequent playback using the Solid-State Recorder (SSR).

## 4. Hardware Calibration and Performance

A detailed baseline calibration was performed for each WBD model (including the Flight Spare) at the unit level.  These unit-level measurements, designed to establish the absolute calibration of the instrument, included amplitude/frequency responses for all filters and conversion modes, noise levels for all bands, characterisation of non-linear effects, and response over temperature.  Each of these calibrations was carried out after final assembly of a given flight model in accordance with a fixed procedure so that any differences in performance from unit to unit could be identified.  Since WBD utilises signals from sensors provided by other experiments (EFW and STAFF), each WBD unit-level calibration was augmented by special WEC-level testing carried out during the WEC flight model integrations performed in Velizy, France.  Finally, in order to provide true end-to-end performance verification of the WBD flight units, additional calibration data were obtained during system level integration/test for comparison with measurements taken earlier.

Various WBD performance criteria were established at the beginning of the hardware design phase, based mainly on the characteristics of signals expected in the regions of the magnetosphere

traversed by the Cluster orbit (see Pedersen *et al.*, this issue). In particular, the expected signal strengths as a function of frequency established requirements for receiver sensitivity and dynamic range.

Based on results from calibration and other testing, the measured performance for the WBD flight models is considered to be excellent, consistent with design goals and predicted capability. In the baseband modes (no frequency conversion) signals of 5 uV ($4 \times 10^{-18}$ $V^2/m^2Hz$, assuming 100 m sphere-to-sphere separation and a bandwidth of 10 kHz) can be detected. In the frequency conversion modes (125 kHz, 250 kHz, 500 kHz) signals of 10 uV ($1.5 \times 10^{-17}$ $V^2/m^2Hz$) can be detected. With the combined receiver and AGC design, signals of 1.5 V can be measured without saturation effects, giving a dynamic range of over 100 dB. Considerable effort went into making the WBD flight units as identical to one another as possible. The result is that frequency/amplitude response characteristics of the WBD flight models are the same to within about 1 dB of accuracy. End-to-end (system level) measurements of the background noise floor are the same to within 2-3 dB. Variations in the background noise floor from unit to unit are attributed to small differences in the EMC environment associated with each individual spacecraft.

### 5. WBD Operations

Although WBD can be commanded to a large number of internal configurations (antenna, bandwidth, gain select, etc.), the most significant WBD operational aspect relates to the manner of telemetry acquisition. Because the wide-band approach carries a basic requirement for high data rates, WBD data (other than housekeeping parameters) do not appear in the low rate telemetry. Rather, two special high-data-rate telemetry acquisition modes were implemented to support WBD operations. As discussed earlier, these are acquisition mode TDA 8, which involves real-time data reception by a DSN ground station, and acquisition mode TDA 5.2, which is a special record mode (BM2) dedicated to WBD. The use of these modes is constrained by various operational considerations, including the availability of appropriate ground-based receiving antennas.

During the Cluster mission, the primary mode for acquiring WBD data will be the single-spacecraft TDA 8 mode of operation using the DSN. By agreement, DSN will provide a minimum of 2 hours of coverage per spacecraft per 57-hour orbit. Also, to avoid interference with ESOC operations, the Madrid DSN station will not be used on a regular basis, since it resides at roughly the same latitude as the ESOC Redu and Odenwald stations. Hence, the bulk of the WBD coverage will be provided by the Canberra and Goldstone DSN stations. Since the TDA 8 mode utilises the entire bandwidth of the downlink, data from the other Cluster experiments must be recorded on the solid-state recorder during the DSN acquisition periods. Multi-spacecraft DSN operations will be performed in support of the interferometry objective discussed earlier. Given the logistical difficulty of the associated scheduling task, these specialised interferometer operations will be carried out relatively infrequently (on the order of 1 hour per month). In the event that simultaneous DSN acquisition using four spacecraft cannot be accomplished due to scheduling or other constraints, the dedicated BM2 record mode will be used. However, since BM2 usage results in the acquisition of only small amounts of data from experiments other than WBD, by agreement BM2 will be used only a few times during the two-year Cluster mission.

Since WBD is part of the WEC, WBD mission operations must take place within the context of WEC operations. As is the case for all aspects of WEC operations, the Joint Science Operations Centre (JSOC) will provide the coordinating interface for DSN scheduling.

## 6. WBD Data-Processing

During the Cluster mission, WBD data are acquired by JPL/DSN at an average rate of about 3 Gbytes per week. These data are placed on 8mm tape cartridges and mailed to Iowa on a timely schedule. A pre-processing step then frame-synchronises the data, resulting in a permanent WBD data archive of original waveforms residing on CD-ROM at Iowa. By agreement, duplicate CD-ROMs are prepared and distributed to the French, British, and Scandinavian Cluster data centres on a regular basis. WBD BM2 data and WBD housekeeping data are contained in the raw data medium CD-ROMs distributed by the Cluster Data Disposition System (DDS).

As discussed in Pedersen *et al.* (this issue), the Interactive Science Data Analysis Tool (ISDAT) is the primary software package used by the WEC for detailed data analysis. For WBD, this requires the development of database handler front-end software so that ISDAT can read the TDA mode 8 and BM2 data. Likewise, ISDAT client application routines that process and display WBD-specific data products are to be completed prior to launch.

## 7. Summary

WBD instruments are included on all four of the Cluster spacecraft. Performance of the wide-band receivers has been determined by test to be very good in terms of both sensitivity and dynamic range, easily meeting design expectations. Although WBD has a relatively low operational duty cycle (~4% of orbit coverage per spacecraft), the WBD waveform measurements are expected to contribute significantly to WEC science, and thereby to the attainment of the Cluster Mission science objectives.

## 8. Acknowledgements

## 9. References

Ashour-Abdalla, M., and C. F. Kennel, Nonconvective and convective electron cyclotron harmonic instabilities, J. Geophys. Res., 83, 1531-1543, 1978.

Baumback, M. M., D. A. Gurnett, W. Calvert, and S. D. Shawhan: 1986, Satellite interferometric measurements of auroral kilometric radiation, Geophys. Res. Lett., 13, 1105-1108.

Gurnett, D. A., R. R. Anderson, F. L. Scarf, R. W. Fredricks, and E. J. Smith, Initial results from the ISEE 1 and 2 plasma wave investigation, <u>Space Sci. Rev.</u>, <u>23</u>, 103-122, 1979.

Gurnett, D. A., A. M. Persoon, R. F. Randall, D. L. Odem, S. L. Remington, T. F. Averkamp, M. M. DeBower, G. B. Hospodarsky, R. L. Huff, D. L. Kirchner, M. A. Mitchell, B. T. Pham, J. R. Phillips, W. J. Schintler, P. Sheyko, and D. R. Tomash:  1995, The Polar Plasma Wave Instrument, <u>Space Sci. Rev.</u>, <u>71</u>, 597-622.

Helliwell, R. A., <u>Whistlers and Related Ionospheric Phenomena</u>, Stanford University Press, Stanford, CA, 1965.

Kennel, C. F., and H. E. Petschek, Limit on stably trapped particle fluxes, <u>J. Geophys. Res.</u>, <u>71</u>, 1-28, 1966.

Kintner, P. M., M. C. Kelley, and F. S. Mozer, Electrostatic hydrogen cyclotron waves near one Earth radius altitude in the polar magnetosphere, <u>Geophys. Res. Lett.</u>, <u>5</u>, 139-142, 1978.

Pedersen, A., *et al.*, 1996 (this issue).

Persoon, A. M., D. A. Gurnett, and S. D. Shawhan, Polar cap electron densities from DE 1 plasma wave observations, <u>J. Geophys. Res.</u>, <u>88</u>, 10,123-10,135, 1983.